Use of nonlinear upconverting nanoparticles provides increased spatial resolution in fluorescence diffuse imaging

Pontus Svenmarker,* Can T. Xu, and Stefan Andersson-Engels

Department of Physics, Lund University, P.O. Box 118, S-221 00 Lund, Sweden
**Corresponding author: pontus.svenmarker@fysik.lth.se*

Received May 6, 2010; revised July 15, 2010; accepted July 15, 2010;
posted July 26, 2010 (Doc. ID 128052); published August 13, 2010

Fluorescence diffuse imaging (FDI) suffers from limited spatial resolution. In this Letter, we report a scanning imaging approach to increase the resolution of FDI using nonlinear fluorophores. The resolution of a linear fluorophore was compared with nonlinear upconverting nanoparticles ($NaYF_4$:Yb^{3+}/Tm^{3+}) in a tissue phantom. A resolution improvement of a factor of 1.3 was found experimentally. Simulations suggested a maximum resolution improvement of a factor of 1.45. Usage of nonlinear fluorophores is a promising method for increasing the spatial resolution in FDI. © 2010 Optical Society of America

OCIS codes: 110.0113, 170.0170, 190.3970, 190.7220, 350.5730.

In recent years, new optical technologies for small-animal imaging have been developed. Macroscopic fluorescence diffuse imaging (FDI) is one of the techniques allowing investigations of whole animals with optical contrast. Together with advances of fluorescent reporter genes, *in vivo* molecular interactions can be visualized and studied dynamically over a prolonged time, without the need to sacrifice the animal [1–3]. Photon migration in tissue is dominated by scattering, making it cumbersome to backtrack the photon path. Tissue scattering also makes it troublesome to focus the photons to a small volume. Hence, optical imaging in tissue intrinsically suffers from limited spatial resolution.

Many attempts to improve on spatial resolution have been made, with the majority using time-gated techniques [4,5]. By looking only at the ballistic light, the photon trajectories straighten and image resolution improves. The same idea has also been applied to fluorescence tomography to improve image quality [6]. It has also been shown that, for fluorescence imaging, raster scanning the excitation source across the object, rather than using wide-field illumination, improves the image contrast [7].

Upconverting nanoparticles have been suggested as a fluorescence marker for biomedical imaging applications. They exhibit the unique property to emit an anti-Stokes shifted photon following absorption of two or more near-IR photons [8]. Recent technological advances have increased their otherwise low quantum efficiency [9] and made them suitable for FDI. Conventional fluorescent dyes have an extremely low two-photon absorption cross section [10], thereby not ideal for FDI, because not enough light intensity can be delivered. Upconverting nanoparticles, however, have through-energy transfer upconversion, a 10 orders of magnitude higher fluorescence efficiency than two-photon absorption [11], thus allowing imaging through several millimeters of tissue. With upconverting nanoparticles, it is also possible to perform autofluorescence insensitive measurements—something that has been demonstrated both for planar imaging [12] as well as tomography [13].

In this Letter, we demonstrate a scanning imaging approach to improve the spatial resolution for FDI using nonlinear fluorophores. The experiments were performed in a well-controlled phantom environment showing an increased resolution using upconverting nanoparticles in comparison to a conventional linear fluorescent dye. Moreover, Monte Carlo photon propagation simulations are presented to show the general trend for resolution improvement at different imaging depths and the excitation beam profile resolution dependence.

Fluorescence imaging in turbid media can be described as a coupled problem, with one part describing the excitation light propagation and another the fluorescence emission propagation. The linear fluorescence emission, F_1, detected at position r_d, with the source placed in position r_s, for volume V, with yield η_l, can be written as

$$F_\mathrm{l}(r_d) = \int_V U_\mathrm{x}(r_s, \mathbf{r}) \eta_\mathrm{l}(\mathbf{r}) U_f^*(r_d, \mathbf{r}) \mathrm{d}V, \qquad (1)$$

where U_x denotes the excitation light propagation and U_f^* is the adjoint fluorescence propagation. Similarly, the nonlinear fluorescence emission F_nl, is given as

$$F_\mathrm{nl}(r_d) = \int_V U_x^\gamma(r_s, \mathbf{r}) \eta_\mathrm{nl}(\mathbf{r}) U_f^*(r_d, \mathbf{r}) \mathrm{d}V, \qquad (2)$$

with η_nl describing the nonlinear fluorescence yield. Note that the fluorescence emission depends on the excitation photon density raised to the power of γ (for quadratic upconverting nanoparticles $\gamma = 2$).

Photon propagation simulations were made to calculate image resolution at different depths for linear and nonlinear fluorophores in a transmission geometry. The nonlinear fluorescence was modeled as the excitation field squared, in agreement with Eq. (2). The simulations assumed a 17-mm-thick homogeneous brick and a 2.4-mm-wide fluorescent inclusion. Laser excitation was modeled as either a pencil beam or a 5 mm FWHM Gaussian beam. The detector was assumed to cover the entire opposite side of the brick. The optical properties at the

excitation wavelength were chosen to have a reduced scattering coefficient of $\mu_s'^{x} = 5.0\ \mathrm{cm}^{-1}$ and an absorption coefficient of $\mu_a^{x} = 0.5\ \mathrm{cm}^{-1}$. At the emission wavelength, the reduced scattering coefficient was $\mu_s'^{f} = 7.5\ \mathrm{cm}^{-1}$ and the absorption coefficient was $\mu_a^{f} = 0.2\ \mathrm{cm}^{-1}$. All photon-density propagation maps were calculated using graphics-processing-unit accelerated Monte Carlo simulations [14].

For a fluorophore depth of 7 mm from the excitation side with the Gaussian beam, a clear spatial resolution improvement could be seen, as presented in Fig. 1(a). The linear fluorophore gave an FWHM of 10.3 mm and the nonlinear fluorophore an FWHM of 7.9 mm—an improvement of a factor of 1.3. Equal spatial resolution improvement could be seen at almost all imaging depths [Fig. 1(b)], hence making it independent to the imaging depth. For the pencil beam, the narrowest beam profile possible, an even further increased resolution improvement of a factor of 1.45 could be observed. The narrower the beam profile is, the higher the resolution improvement will be, owing to the quadratic excitation density dependence. At imaging depths more shallow than the mean free path, here 2 mm, no resolution improvement was gained owing to the limited photon scattering. At these distances, there is no difference between the photon-density distribution for the linear and nonlinear case.

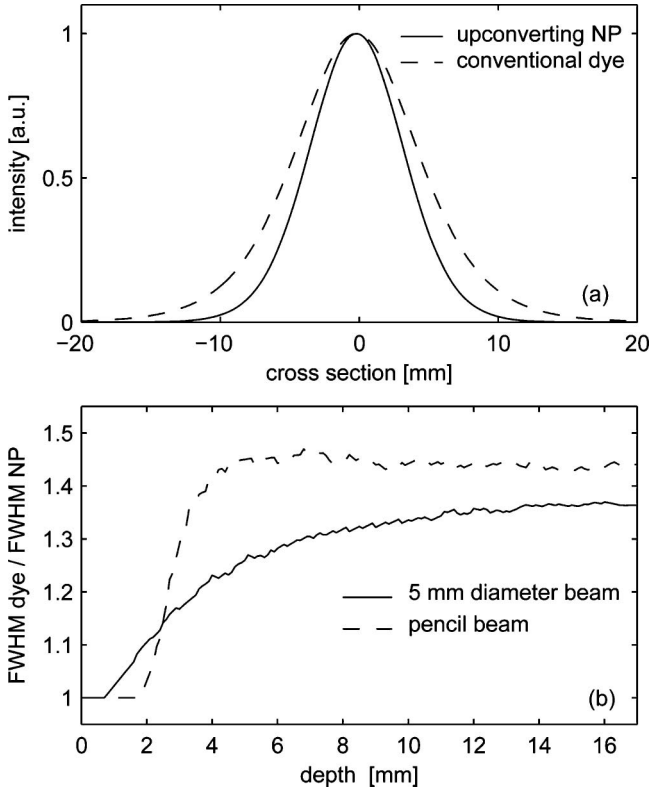

Fig. 1. Monte Carlo simulation of light propagation modeling the resolution using the scanning imaging method for upconverting nanoparticles and conventional linear fluorescent dyes: (a) image cross section for a transmission geometry with the fluorophore located at a 7 mm depth from the excitation side, (b) ratio of the FWHM of the linear fluorescent dye to the FWHM of the upconverting nanoparticles versus depth locations of the simulated rod inclusion.

Two cylindrical tissue phantoms with the same thickness of 17 mm consisting of water, intralipid, and ink were prepared. To ensure a fair comparison of the image resolution, the concentrations of the intralipid and the ink were set to obtain similar optical properties at both excitation wavelengths, 785 nm and 975 nm, respectively. Time-of-flight spectroscopy [15] measured the optical properties to a reduced scattering coefficient of $\mu_s'(785\ \mathrm{nm}) = 5.1\ \mathrm{cm}^{-1}$, $\mu_s'(975\ \mathrm{nm}) = 5.0\ \mathrm{cm}^{-1}$ and an absorption coefficient of $\mu_a(785\ \mathrm{nm}) = 0.52\ \mathrm{cm}^{-1}$, $\mu_a(975\ \mathrm{nm}) = 0.57\ \mathrm{cm}^{-1}$.

Imaging was done with the system depicted in Fig. 2. Collimated diode lasers, delivering no more than 80 mW, were used to illuminate the phantom from below in a transmission geometry with a spot size of 5 mm in diameter. An electron multiplying CCD, a 50/1.4 mm imaging lens, and a set of interference filters centered at 800 nm were used to detect the fluorescent light.

A glass tube with an inner diameter of 2.4 mm was used to hold the nonlinear as well as the linear fluorophore. It was submerged into the liquid phantom to a depth of 7 mm from the excitation side. The linear fluorophore used (Dy-781, Dyomics GmbH) was dissolved in ethanol to a concentration of 1 μM and excited at 785 nm. The nonlinear fluorophore used was upconverting nanoparticles ($NaYF_4$:Yb^{3+}/Tm^{3+}) dispersed in dimethyl sulfoxide to a concentration of 1 wt.% and excited at 975 nm.

Images were captured by raster scanning the laser in a grid pattern. In total, 160 points were used, distributed in four rows with 40 points in each row. For each position of the laser, the emitted fluorescence from the entire side of the phantom was measured and summed to make up one

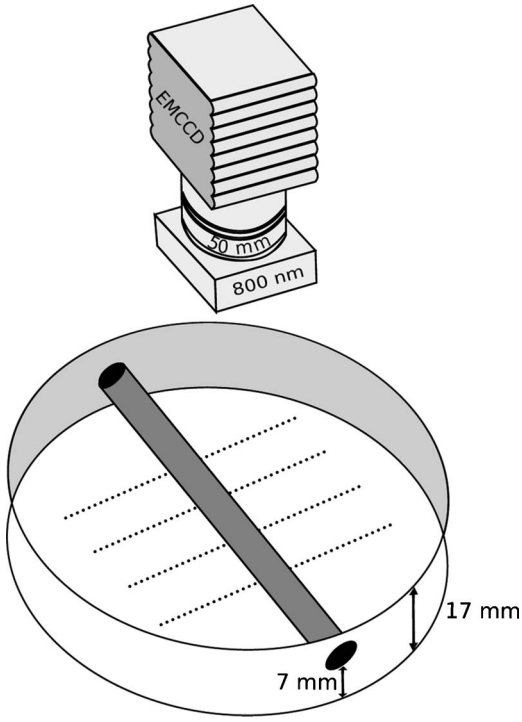

Fig. 2. Schematic of the experimental setup. The excitation laser was scanned in four rows according to the black dots indicated. One fluorescent rod was submerged into a tissue phantom. Fluorescence was collected through the 800 nm bandpass filter and recorded by a camera.

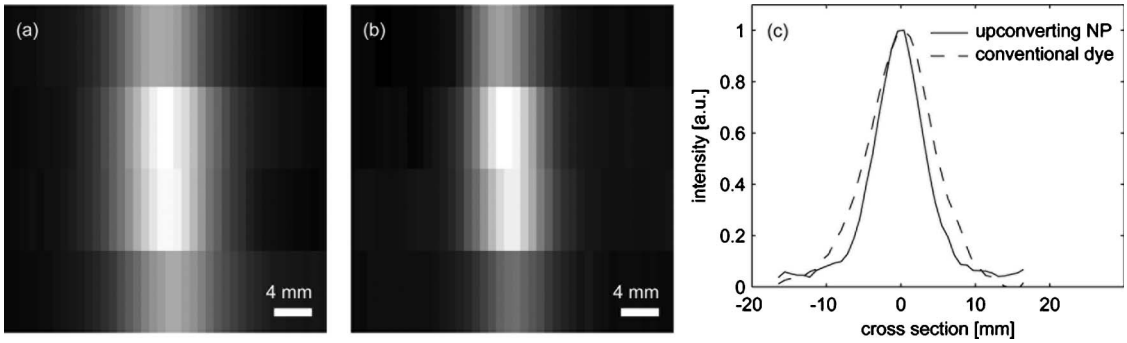

Fig. 3. Fluorescence images using the scanning imaging technique. Each pixel in the image correspond to the fluorescence induced by a single excitation point. Here the excitation source was scanned in a 40×40 grid, thus generating an image of 40×40 pixels. (a) Linear conventional fluorescence dye, (b) upconverting nanoparticles. A cross section of images (a) and (b) is displayed in (c).

pixel in the image. Hence the number of pixels in the image was given by the number of excitation positions and not by the number of camera pixels. The resolution is thus determined by the photon density of the excitation light and not by the photon density of the fluorescence emission light. In this way, because the two-photon density is more narrow than the single-photon density distribution, the resolution could be increased. Figure 3 shows the images for a linear conventional fluorescent dye and nonlinear upconverting nanoparticles. The cross-section profiles show the FWHM as 10.5 mm and 8.0 mm, respectively, for the fluorescent dye and the upconverting nanoparticles, giving an improvement of a factor of 1.3.

In diffuse imaging, the spatial resolution depends on the optical properties. Decreased scattering and increased absorption will both result in a higher spatial resolution. Therefore, it was important to keep the optical properties at the two excitation wavelengths, 785 nm and 975 nm, equal to make a fair comparison of the resolution. In biological tissue, the slightly lower scattering and higher absorption at 975 nm as compared to 785 nm, will most likely result in a more profound enhancement of the spatial resolution. Moreover, the image resolution improvement was found independent of the imaging depth. The theoretical simulations agreed well with the experimental data, both suggesting a resolution improvement factor of 1.3. For the simulations, assuming a pencil beam, the resolution improvement factor could be increased to 1.45. This can be viewed as the theoretical maximum resolution improvement obtainable.

In conclusion, we present and demonstrate a method for increasing the spatial resolution of diffuse fluorescence imaging by exploiting the nonlinear excitation dependence of upconverting nanoparticles.

The authors gratefully acknowledge Zhiguo Zhang and his group at the Harbin Institute of Technology and Gabriel Somesfalean for the generous donation of the upconverting nanoparticles. This study was supported by a Linnaeus grant by the Lund Laser Centre.

References

1. V. Ntziachristos, Annu. Rev. Biomed. Eng. **8**, 1 (2006).
2. V. Ntziachristos, J. Ripoll, L. V. Wang, and R. Weissleder, Nat. Biotechnol. **23**, 313 (2005).
3. A. H. Hielscher, Curr. Opin. Biotechnol. **16**, 79 (2005).
4. S. Andersson-Engels, R. Berg, S. Svanberg, and O. Jarlman, Opt. Lett. **15**, 1179 (1990).
5. L. Wang, P. P. Ho, C. Liu, G. Zhang, and R. R. Alfano, Science **253**, 769 (1991).
6. M. J. Niedre, R. H. de Kleine, E. Aikawa, D. G. Kirsch, R. Weissleder, and V. Ntziachristos, Proc. Natl. Acad. Sci. USA **105**, 19126 (2008).
7. B. W. Pogue, S. L. Gibbs, B. Chen, and M. Savellano, Technol. Cancer. Res. Treat. **3**, 15 (2004).
8. S. Heer, K. Kompe, H. U. Gudel, and M. Haase, Adv. Mater. **16**, 2102 (2004).
9. G. S. Yi and G. M. Chow, Chem. Mater. **19**, 341 (2007).
10. C. Xu and W. W. Webb, J. Opt. Soc. Am. B **13**, 481 (1996).
11. F. Auzel, Chem. Rev. **104**, 139 (2004).
12. C. T. Xu, N. Svensson, J. Axelsson, P. Svenmarker, G. Somesfalean, G. Chen, H. Liang, H. Liu, Z. Zhang, and S. Andersson-Engels, Appl. Phys. Lett. **93**, 171103 (2008).
13. C. T. Xu, J. Axelsson, and S. Andersson-Engels, Appl. Phys. Lett. **94**, 251107 (2009).
14. E. Alerstam, T. Svensson, and S. Andersson-Engels, J. Biomed. Opt. **13**, 060504 (2008).
15. E. Alerstam, S. Andersson-Engels, and T. Svensson, Opt. Express **16**, 10440 (2008).